Plastic antibody for the electrochemical detection of bacterial surface proteins

M. Azizur R. Khan, Felismina T.C. Moreira, Jordi Riu, M. Goreti F. Sales

A B S T R A C T

This work presents a novel molecularly imprinted polymer (MIP) for the indirect detection of bacteria, by targeting an outer membrane protein on a disposable device. Protein A (PA) was selected for this purpose, as a representative protein of the outer surface of *Staphylococcus aureus*. The imprinted polymer was assembled directly on a film of single walled carbon nanotubes (SWCNTs), placed on screen-printed electrodes (SPEs). The MIP material was produced by electropolymerizing 3-aminophenol in the presence of the protein template (PA) using cyclic voltammetry (CV). The proteins entrapped at the polymeric backbone were digested by the action of proteolytic activity of proteinase K and then washed away to create vacant sites.

The performance of the corresponding imprinted and non-imprinted electrodes was evaluated by EIS and the effect of several variables, such as monomer and template concentrations, or thickness of imprinting surface, was controlled and optimized by the number of CV cycles. The detection limit of the MIP-based sensors was 0.60 nM in MES buffer. High repeatability and good selectivity were observed in the presence of a model protein BSA. The sensor performance was also tested to check the effect of inorganic ions in tap water. The detection limit observed was 16.83 nM, with a recovery factor of 91.1 ± 6.6%. The sensor described in this work is a potential tool for screening PA on-site, due to the simplicity of fabrication, disposability, short response time, low cost, good sensitivity and selectivity.

Keywords:
Plastic antibody
Molecularly imprinted polymer
Electropolymerization
Bacterial surface proteins
Staphylococcus aureus
Screen-printed electrodes
Disposable device

1. Introduction

In our daily life, diseases and productivity losses caused by bacteria are very common, and *Staphylococcus aureus* (*S. aureus*) is the responsible for a spectrum of pathologic conditions, including circumscriptive suppurations, bloodstream invasion, a variety of toxic syndromes, and serious skin diseases [1]. *S. aureus* can produce several types (A, B, C, D, and E) of enterotoxins that cause gastroenteritis [2,3]. The presence of the bacterium in water is also a health hazard if the water is held at a temperature that allows bacterial growth, which permits synthesis of enterotoxins. Not surprisingly, *S. aureus* has several virulence factors including cytotoxic hemolysins, leukocidins, enterotoxins, teichoic acid, and protein A [1].

Protein A (PA) is a cell wall constituent [4] of S. *aureus* and is covalently linked to the peptidoglycan structure of the bacterium. Around 99% of S. *aureus* strains have PA on the cell wall [5] and between 8 and 30% of it is secreted during the exponential growth phase [6,7]. This extracellular protein can thus be detected and it can be used as an indicator of the presence of the microorganism in clinical or food specimens [5,8]. In this context, the detection of protein A is of great importance and may constitute a simple way to detect the presence of *S. aureus* in a given sample.

Surface proteins of pathogenic bacteria can serve as protective antigens and malignity markers, though they can be technically challenging to detect. Several biochemical and microbiological techniques have been employed to detect bacterial surface proteins, including fluorescent labeling [9], stable isotope labeling [10], LC–MS coupled biotinylation [11], surface shaving approaches [12], genome analyses and protein and antibody arrays [13] or enzyme-linked immunosorbent assay (ELISA) [14]. The antigen/antibody reaction is highly preferred in this context due to the high selectivity of the affinity reaction taking place between these biomolecules. However, the use of natural antibodies for protein detection is

expensive due to the high cost of the material, the need for special handling and storage, and the poor stability of the antibodies.

These constraints would be overcome by replacing natural antibodies by artificial receptors such as molecularly imprinting polymers (MIPs), also known as plastic antibodies [15,16]. Although the development of MIP materials is a technology from the 70s, protein and/or microorganism imprinting has faced many difficulties within time [17–21]. Few reports have been published for microorganism detection based on stamp imprinting. The most remarkable ones need a pre-polymerization step to make a gel which can be then deposited by a controlled way over the electrode surface [22–24]. The detection technique used is QCM (quartz crystal microbalance) [22,23] which is limited by externally induced mechanical vibrations and large overall footprint, and heat flow measurements [24] which could be limited by temperature control. But most of the MIP materials obtained so far are used for separation and binding [25], and the detection of protein based on imprinted materials is not so much explored yet, although it remains as a promising field [18–21]. As far as we know molecular imprinting-based bacterial surface protein detection is still now missing.

In MIPs, a polymeric network is assembled (2-D or 3-D) and molded around a suitable template molecule (i.e. the target analyte), which upon removal [26–28] yields nano/micro cavities of specific size, shape, and/or chemical functionality in a matrix. Such molecularly designed cavities show affinity for the imprinted molecule over other structurally and chemically related compounds. Preparation of thin films by this method is very attractive for chemical and biological sensing applications, due to long term stability with respect to pH or temperature changes. Several strategies have been used for the fabrication of MIPs, such as vinyl-based [26] or sol-gel polymerizations [27], that are chemically or physically initiated/sustained (i.e., by electromagnetic radiation or and electrical stimulus) [28]. Any of these may be achieved by surface imprinting (2-D) and bulk imprinting (3-D). Usually electrochemical imprinting offers the advantage of controlling the thickness of the imprinting layer easily, by adjusting the time or the number of cycles during polymerization. Electrochemical MIPs preparation is also a green synthesis process, since it is made without using any type of free radical formation agent [29], as most of the conventional polymerization processes. Between the 3-D and 2-D electrochemical imprinting, the former offers a higher number of rebinding positions, while needing less optimization procedures to control the surface polymerization thickness (which is the crucial part of the imprinting stage in surface imprinting).

The production of an electropolymerized MIP film is however confined to the existence of suitable monomers. Many monomers have been used so far for this purpose [29]. In this regard, and having in mind that a protein is being targeted, aminophenol would be a good choice. The growth of an electropolymerized aminophenol film is self-limiting, and therefore its thickness may be easily controlled [28]. Furthermore, the presence of amino groups at the imprinting polymeric matrix would attract the target protein by permselectivity during the sensing stage which would presumably contribute to an increased sensitivity and better detection ability.

In this paper, we used electrochemical bulk imprinting (3-D) for the fabrication of MIPs over single walled carbon nanotubes-based disposable screen printed electrodes (SWCNT-SPEs) for PA detection. The PA from the outer surface of *S. aureus* was mixed with 3-aminophenol monomers and electropolymerized by cyclic voltammetry to entrap PA in the polymeric backbone. PA was removed in a later stage by proteolytic activity of proteinase K and subsequent electrochemical washing by cyclic voltammetry. Electrochemical impedance spectroscopy (EIS) was employed to follow the changes in the electrical features of the working electrode as well as to detect PA with high selectivity and precision.

2. Experimental section

2.1. Apparatus

The electrochemical measurements were conducted with a potentiostat/galvanostat from Metrohm Autolab and a PGSTAT302N (Utrecht, The Netherlands), equipped with a FRA module and controlled by Nova software. The SWCNTs-SPEs were purchased from DropSens (Oviedo, Spain), and composed by a working electrode made of carboxylated SWCNTs, a counter electrode made of carbon and a reference electrode made of silver; electrical contacts were also made of silver. The diameter of the working electrode was 3.80 mm. The SWCNTs-SPEs were connected to a portable switch box, also from DropSens (DRP-DSC), allowing their interface with the potentiostat/galvanostat.

Fourier transform infrared spectroscopy (FTIR) measurements were performed using a Thermo Scientific Smart iTR Nicolet iS10, coupled to a SAGA smart accessory, also from Thermo Scientific (Waltham, USA). Raman measurements were performed in a Thermo Scientific DXR Raman spectrometer with confocal microscopy (Waltham, USA), with a 10 mW 532 nm excitation laser. Images of the materials were taken with an Environmental Scanning Electron Microscope (ESEM) FEI Quanta 400FEG.

2.2. Reagents

All chemicals were of analytical grade and water was de-ionized or ultrapure Milli-Q laboratory grade. Potassium hexacyanoferrate III, potassium hexacyanoferrate II trihydrate, and sodium acetate anhydrous were obtained from Riedel-deHäen; bovine serum albumin (BSA), and proteinase K from Fluka; 3-aminophenol (AP) 99%, and 2-(*N*-morpholino)ethanesulphonic acid monohydrate 98% (MES) from Alfa Aesar; PA(from *S. aureus*) from Sigma Aldrich; and potassium chloride (KCl) from Merck.

2.3. Solutions

Stock solutions of 2.38×10^{-5} mol/L PA were prepared in HEPES buffer (1.0×10^{-4} mol/L, pH 5.0). Standards were obtained by accurate dilution of the previous solution in MES buffer (1.0×10^{-2} mol/L, pH 5.0, KCl 0.1 M) or in sodium acetate buffer (1.0×10^{-2} mol/L, pH 5.0) depending on the study. Electrochemical assays were performed with 5.0×10^{-3} mol/L $[Fe(CN)_6]^{3-}$ and 5.0×10^{-3} mol/L $[Fe(CN)_6]^{4-}$ prepared in MES buffer. The selectivity study was made by a competitive assay in MES buffer and using BSA in a concentration of 7.1×10^{-7} mol/L.

2.4. Electrochemical synthesis of molecular imprinted (MIP) and non-imprinted polymer (NIP) films

Prior to electropolymerization, the SWCNTs-SPEs were cleaned by chronoamperometry (1.7 V, for 60s, in KCl 0.1 M solution) and later stabilized by cyclic voltammetry (−0.2 to 0.8 V, 10 cycles, 50 mV/s, in MES buffer). Then, 75 μL of a solution containing PA 2.38×10^{-6} mol/L and AP 1.0×10^{-2} mol/L in acetate buffer pH 5.0, was casted onto the SPE to cover the three electrodes and polymerization was performed by CV (between −0.2 and 0.8 V at a scan rate of 50 mV/s) for a variable number of cycles. The resulting film was thoroughly washed with de-ionized water and incubated next in proteinase K (500 μg/mL in PBS pH 7.4) for 2.5 h at room temperature. The surface was then washed thoroughly with Milli-Q water and subjected to electrochemical cleaning by 25 CV cycles in MES

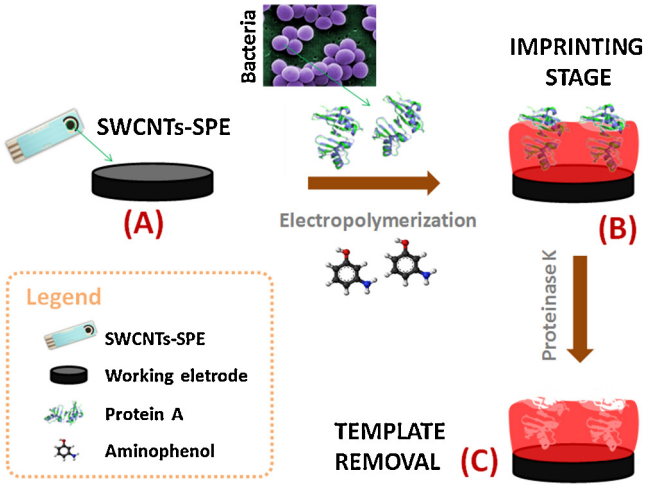

Fig. 1. Schematic representation of the synthetic process. (A) Working area of SWCNTs-SPE; (B) Imprinting stage after electropolymerization of AP along with PA and (C) Binding site formation after template removal by proteinase K.

buffer (potential range −0.2 to 0.8 V, scan rate 0.05 V/s). The overall process has been presented schematically in Fig. 1.

In parallel, non-imprinted polymers (NIPs) have been synthesized in a similar mode, but without presence of PA. Therefore NIPs are similar than MIPs but without the cavities for the target analyte.

2.5. Qualitative characterization of the films

All qualitative analyses were directly performed on the SPE without any treatment. MIP films with PA and after PA removal with proteinase K treatment, and NIP films at different stages of fabrication were analysed by Raman spectroscopy, where the average signal-to-noise ratio (peak height/RMS noise) was set automatically along 5 min of maximum measuring time, for a 5 mW laser power on the sample, and 50 μm slit aperture. FTIR analysis was performed before and after the electropolymerization of MIP and NIP film formation. The FTIR (from 400 to 4000 cm^{-1}) number of scans was set to 256, the resolution to 8, apodization of Happ-Genzel, Mertz Phase correction, and a background gain of 8. ESEM analysis was done at high vacuum and 1×10^5 magnification at 15 kV.

2.6. Binding isotherm

The adsorption dynamics of MIPs and NIPs were studied by incubating increasing concentrations of PA standards, prepared in MES buffer, ranging from picomolar to micromolar level. The incubation time was set to 20 min at room temperature before adding the redox probe for subsequent EIS measurements.

A Langmuir isotherm model (equation 1) was applied to the experimental data, where R_{ct} is the normalized charge transfer-density (kΩ/cm^2), S the concentration of PA (in M) and $R_{ct}{}^{máx}$ is the maximum charge transfer density observed (kΩ/cm^2).The apparent dissociation constant (K_D in M) and the maximum binding capacity ($R_{ct}{}^{máx}$) were calculated from the fitting of the experimental data to the model in equation 1. K_D is the protein concentration required to provide half of the maximum response produced by the device.

$$R_{ct} = \frac{R_{ct}^{máx}}{1 + K_D/[S]} \quad (1)$$

2.7. Electrochemical assays

The redox probes in all CV and EIS measurements were 5.0 mmol/L $[Fe(CN)6]^{3-}$ and 5.0 mmol/L $[Fe(CN)6]^{4-}$ prepared in MES buffer at pH 5.0. In CV assays, the potential ranged from −0.5 to +0.7 V with a scan rate of 50 mV/s. In EIS, an open circuit potential was set using a sinusoidal potential perturbation of 0.01 V amplitude and 50 frequency values logarithmically distributed over a frequency range of 0.1 – 100 kHz.

Calibration curves were performed by EIS measurements for PA in the range from 23.8 pM to 4.76 μM level. At each concentration level, 10 μL of PA standard solution in MES buffer was exposed to the imprinted sensors for 20 min at room temperature. The values of precision corresponded to the standard deviation of triplicate experiments. Selectivity studies were conducted by checking the response of a PA 7.1×10^{-7} mol/L solution prepared in MES buffer at pH 5.0, with or without BSA (7.1×10^{-7} mol/L). Real sample analysis was done by spiking PA in tap water diluted with MES buffer (1:3, tap water/buffer).

3. Results and discussion

3.1. Electropolymerization and imprinting stage

For a successful imprinting, the selection of the polymer has an important role depending on several parameters, such as the degree of polymerization, the selected potential for electropolymerization, and the functional groups of the polymer with ability to increase permselectivity. Polyaminophenol (PAP) exhibits several advantages, including an easy control of the polymer thickness due to a self-limiting growth, and a high degree of permselectivity [30]. The amine and hydroxyl functional groups linked to the aromatic ring may also contribute to establish electrostatic interactions with the target protein at the rebinding event, thereby contributing for its stability at the rebound position, even after washing.

The electropolymerization was established by imposing consecutive CV cycles over the clean-SPE. In the first cycle, the current increased in the direction of the oxidation potentials, evidencing a peak at around 0.6 V. This peak indicated the oxidation of AP, thereby allowing the occurrence of electropolymerization (Fig. 2A). In the reverse scan, down to negative potentials, no peak was present showing the irreversibility of the reaction. The subsequent CV cycles showed a continuous decrease in the current of the system, which confirmed the growing of a non-conductive layer.

The CV profiles of the iron redox probe obtained for the SPE coated with the polymeric film (MIP or NIP) on top of the working electrode clearly confirmed the presence of a highly *blocked* surface (Fig. 2B). The redox peaks of the iron probe at the clean SPEs almost disappeared after formation of the polymeric layer. This was coupled with a higher peak-to-peak potential separation, also evidencing that the surface was *blocked*.

The electrical changes occurring at the SPEs by polymerization were also followed by EIS. In general, the electrochemical properties occurring at the electrode-solution interface were related to simplified Randles cell [31,32]. The circuit consisted of one resistor (solution resistance, R_s) in series with one parallel circuit comprised of a resistor (charge transfer resistance, R_{ct}) and a capacitance of double layer (C_{dl}) (inset, Fig. 2C) [31,33,34]. In this circuit, the Nyquist plot consists of a single semicircle. Such semicircle intersects the real axis (Z′) in two spots: the data point closest to the origin indicates the resistance value of the solution (R_s), while the intercept farthest from the origin indicates the total resistance ($R_{ct} + R_s$). Thus, the charge transfer resistance (R_{ct}) corresponds to the diameter of the observed semicircle. The clean SPE showed very little R_{ct} value, when compared to the polymeric modifications of

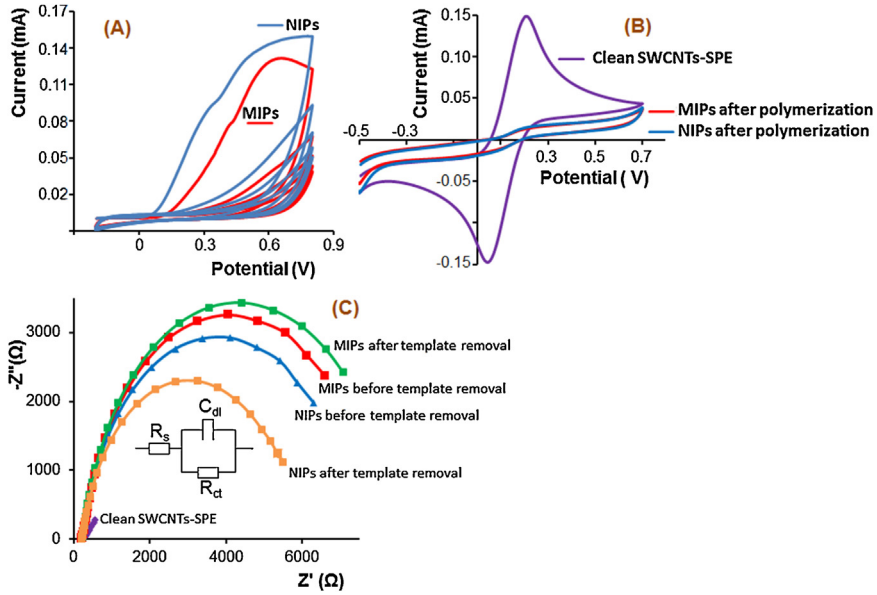

Fig. 2. (A) Electrochemical synthesis of MIPs and NIPs. Electrochemical control of the subsequent modification steps in 5.0 mM $[Fe(CN)_6]^{3-}$ and 5.0 mM $[Fe(CN)_6]^{4-}$, in MES buffer pH 5, carried out by (B) CV and (C) EIS (Nyquist plots) assays for MIPs/NIPs, and Randles circuit (inset).

the surface. As may be seen in Fig. 2C, the polymer on the surface cause a huge increase of the charge-transfer resistance of a clean SPE. This was due to the non-conductive properties of the PAP.

In parallel, the control film (NIP) was synthesized without the presence of PA during electropolymerization. The NIP polymer yielded a lower R_{ct} compared to MIP (Fig. 2C), and this difference could only be attributed to the presence of PA in the MIP polymerization stage. As PA was within the growing polymer, two interrelated events occur: the presence of PA on the matrix changes the electrical properties of the surface where the polymer is growing (when compared with AP growing alone in NIP), which is turn affects the polymer growth as the polymer is being formed by an electrical stimulus applied to the electrode surface. In other words, the differences reflect the direct impact of the protein on the electrical properties of the surface and its indirect impact by promoting a differentiated polymer growth by such different electrical features.

3.2. Protein removal

PA biomolecules hanging at the surface of the imprinted polymer, and exposed to the solution, were removed as peptide fragments by the proteolytic activity of proteinase K. The protein removal changed the typical electrical features of the redox probe, as this additional element no longer existed at the surface. The changes of charge transfer resistance (R_{ct}) are different in MIPs and NIPs after the action of proteinase K and the electrochemical cleaning (Fig. 2C).

When the NIP material was subject to proteinase K, the R_{ct} value of the iron redox probe decreased significantly. This was most probably related to the partial loss of polymer along this process, as no protein existed to be digested. In this case, the enzyme could have partially digested the polymer lying at the surface, because one of its predominant sites of cleavage is peptide bonds near aromatic amino acids with blocked alpha amino groups, and the PAP is likely to have many nitrogen and oxygen related groups linked to aromatic groups.

But the MIP material increased its R_{ct} value after proteinase K action. In a first glance, this seemed a strange behavior, because the enzyme decreased the R_{ct} of the control polymer and protein removal generally decreases the resistance of a given surface. However, the effect of a given protein also depends of its protonation, compared to the redox probe. If PA would be positively protonated, the concentration of the iron redox probe at the surface could increase by ionic interaction, thereby reducing the R_{ct}, despite the fact that a higher amount of a non-conductive compound existed at the surface. Indeed, this was verified in practice, when different concentrations of PA were incubated at the surface of a blank electrode and the resistance decreased. Thus, the increase of the R_{ct} in the MIP layer after protein removal was a combination of opposite events: a decrease caused by polymer loss and an increase caused by protein loss.

3.3. Follow-up of the surface modification

3.3.1. Raman spectroscopy

Raman spectra were recorded for MIP and NIP materials at different stages of the assembly of the sensing surface. The spectra obtained are shown in Fig. S1 (Supplementary Information), displaying the typically observed G and D bands of carbon-based materials.

The I_D/I_G ratio of the clean SWCNTs-SPE was 0.658. After polymerization without template (NIPs), the I_D/I_G ratio changed to 0.738 and after formation of MIPs the I_D/I_G ratio was 0.755. Overall, an increase in the defect band D was observed after polymerization, suggesting the modification of SWCNTs with a less organized carbon material, and this change was not the same in MIPs than in NIPs, accounting for the presence of the protein. Interestingly, after the template removal by the proteolytic activity of proteinase K, the I_D/I_G ratio decreased to 0.724 for MIPs. In the case of NIPs, after the action of proteinase K (in this case there was no template to remove) the I_D/I_G ratio was 0.735, almost similar to the ratio without the action of proteinase K. The difference in the I_D/I_G ratio for MIPs before and after the template removal, and the quasi constant values in the I_D/I_G ratio for NIPs before and after the template removal, is a strong evidence of the successful imprinting.

3.3.2. Fourier transformed infrared spectroscopy

The AP electropolymerization is expected to yield polymers which contain phenyl, quinoid and benzenoid ring [35–37] and the FTIR analysis was conducted directly over the SPEs directly

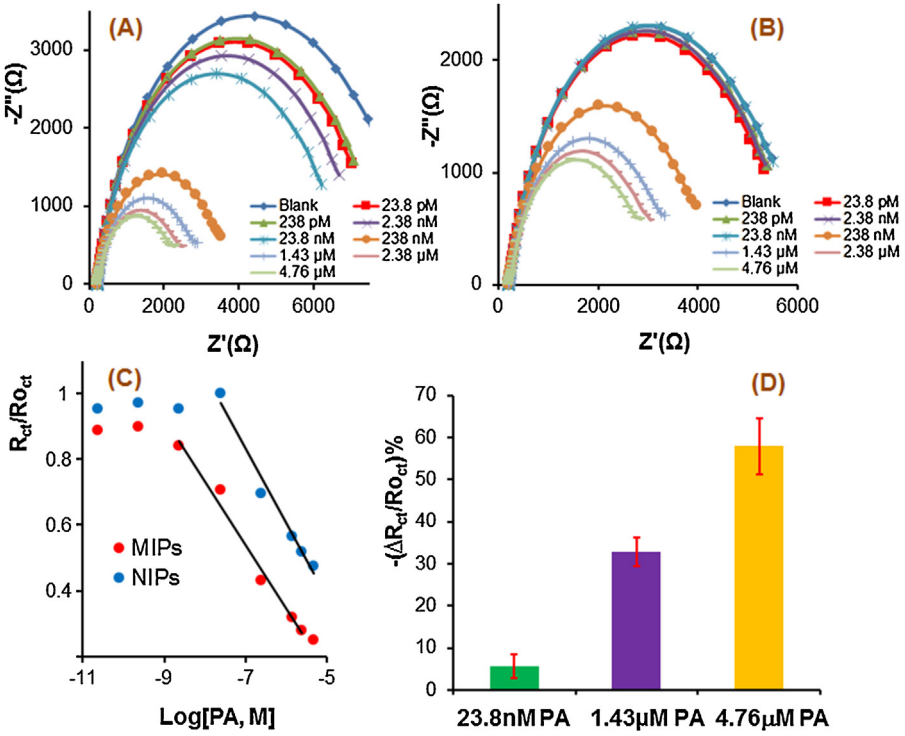

Fig. 3. EIS measurements of (A) MIPs and (B) NIPs based sensors and the corresponding calibration curves (C) in 5.0 mM $[Fe(CN)_6]^{3-}$ and 5.0 mM $[Fe(CN)_6]^{4-}$, in MES buffer pH 5, with different concentrations of PA; (D) Precision of MIPs-based device. The error bars correspond to ± the standard deviation of the three results.

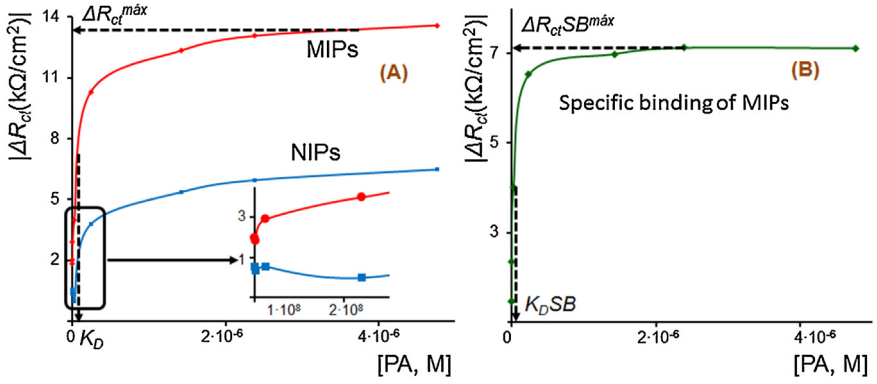

Fig. 4. Graphical representation of the Langmuir isotherm plot: (A) comparison of signal density and maximum binding capacity ($\Delta R_{ct}{}^{máx}$) of MIPs and NIPs; (B) Binding isotherm of MIPs after subtracted NIPs signal density.

over the SPEs at before and after polymerization of sensors fabrication to find out their existence. The results are presented in Fig. S2 (Supplementary Information).

After polymerization, the MIPs and NIPs showed a characteristic broad peak at ~3000–3700 cm^{-1} for the N—H and O—H stretching in the polymeric network, which is absent in the clean SWCNTs-SPEs. The peak position also changed from 1571 cm^{-1} (clean SWCNTs-SPE) to 1589 cm^{-1} (after polymerization) with high intensity and broad peak, which is the indication of a mixture of the C=C and C=N stretching vibrations in the quinoid ring.

3.3.3. Electron microscopy

The surface morphology was investigated by environmental scanning electron microscope at different stages of the MIP fabrication. The collected images are presented in Fig. S3 (Supplementary information). The clean SWCNTs-SPE evidenced the presence of carbon nanotubes well distributed within the carbon structure and several pores of different sizes, randomly distributed over the surface. Such porous surface disappeared after assembling the MIP layer on top of SWCNTs; the microscopic image of the MIP evidenced a compact structure, with no pores and, apparently, homogenous. After the template removal, the surface of MIP materials evidenced several pores, of small dimension. In addition the MIP surface became more rough which could indicated the exit of oligomer fractions of the polymer and/or polymer degradation derived by the enzymatic action.

3.4. Analytical performance of the sensor

The analytical performance of the sensor was evaluated by incubating the sensing surface (MIP or NIP) with a PA standard solution of increasing concentration. For this purpose, a drop of standard solution was casted on top of the working electrode and let stand there for 20 min. During this period, PA rebinding was allowed. After this, the electrode surface was washed and the three electrode

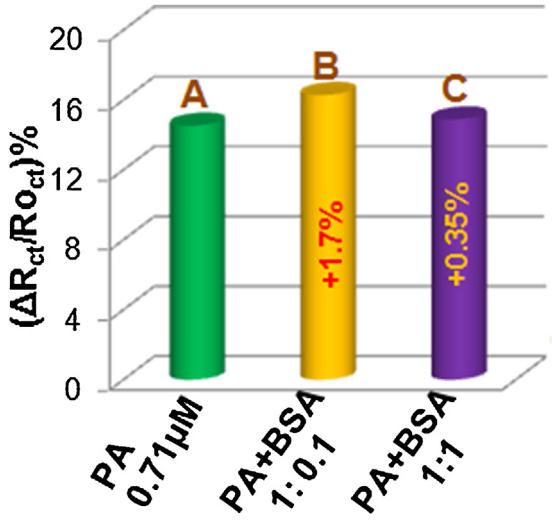

Fig. 5. Selectivity test of the sensor by competitive method; signal for (A) only PA, (B) mixture of PA and BSA 1: 0.1 (in M), and (C) mixture of PA and BSA 1: 1 (in M).

system of the SPE covered with the standard iron redox probe for electrical reading.

Fig. 3 shows the EIS detection (ranging from pmol L^{-1} to μmol L^{-1}) recorded for MIP and NIP-based electrodes. Fig. 3A and B showed the impedance responses upon the addition of different PA concentrations for the MIP and NIP-based devices respectively. Both MIP and NIP devices displayed decreasing charge-transfer resistances when the PA concentration increased (Fig. 3A and C). This lowering of R_{ct} with increasing PA concentration was probably related to the positive protonation of the imprinted surface by the interaction of PA with the amino or hydroxyl groups of the imprinted polymers, under the conditions in which the assay was performed. The imprinted polymer contains —NH and —OH groups (FTIR in Fig. S2 of the Supplementary Information), and probably the electrostatic interaction of these groups with the PA functional groups create protonation over the imprinted surface. Such interaction between PA and MIP increased the density of positive charges over the receptor surface, which in turn increased the number of negatively charged iron redox probe molecules attracted over the surface.

For low level concentrations (up to 23.8 nM) the NIP-based devices presented a random behaviour against increasing protein A (PA) concentrations (Fig. 3B and C). For higher concentrations, the NIP R_{ct} values start to decrease, thereby confirming the existence of non-specific binding of PA to the receptor surface. The MIP surface displayed a similar behaviour, but the linear response was extended over a wider range of PA concentrations, including lower concentrations of protein.

The detection limit (LOD) of MIPs was 0.60 nM, considering three times the standard deviation of the blank response. The precision of the MIP-based devices (results based on three different measurements using three different devices), at different levels of concentration is shown in Fig. 3D.

3.5. Binding isotherm

The isotherm based on EIS results of MIPs follows a hyperbolic response (Fig. 4A) approaching the typical behaviour of antibody/antigen interactions [34]. The parametric data over the Langmuir equation ($\Delta R_{ct}^{máx}$ and K_D, in Eq. (1) assesses the performance of the sensor in terms of template rebinding. $\Delta R_{ct}^{máx}$ reflects the differences in the amount of PA bound to the sensor surface and K_D (the dissociation constant) shows the concentration of PA providing half of the maximum response ($\Delta R_{ct}^{máx}$), thus measuring how well PA form complexes with MIPs and the affinity with which it occurs. If the K_D is low it indicates a large binding affinity, as there action will approach the maximum response more rapidly. On the contrary, a high K_D indicates that the sensor does not efficiently bind with PA.

In general, the MIP $\Delta R_{ct}^{máx}$ and K_D values should be distinguishable from control NIPs. R_{ct} and Ro_{ct} respectively indicates normalized and baseline charge transfer resistance of the sensor, and hence the signal density ΔR_{ct} (where $\Delta R_{ct} = R_{ct}\text{-}Ro_{ct}$) represents the binding adsorption for each concentration of PA. The signal density (ΔR_{ct} *per* unit area of electrode) for MIPs increases after each addition of PA (until a saturation) whereas for NIPs the signal density is scattered at low concentration and it suffers from non-specific binding at high concentration of PA (Fig. 4A). $\Delta R_{ct}^{máx}$ for MIPs is 13.34 kΩ/cm^2 and for NIPs is 6.21 kΩ/cm^2 ($\Delta R_{ct}^{máx}$ of MIPs is 2.15 times higher than the NIPs one). The dissociation constant (K_D) is 119 nM for MIPs. NIPs showed a random affinity at low concentration of PA (inset in Fig. 4A) whereas the MIP signal density was regularly increasing over all the range of concentrations. The most interesting information from the binding isotherms is found after subtracting the NIP signal density from the MIP signal: the subtracted signal density ΔR_{ct}SB (where $\Delta R_{ct}\text{SB} = \Delta R_{ct\,\text{MIP}} - \Delta R_{ct\,\text{NIP}}$) also follows a hyperbolic response (Fig. 4B) which reflects the amount of specific binding that occurs with MIPs without considering non-specific binding. The dissociation constant for the specific binding (K_DSB) of MIPs is 23.8 nM with maximum specific binding ($\Delta R_{ct}\text{SB}^{máx}$) of 7.12 kΩ/$cm^2$ what shows the difference between MIPs and NIPs.

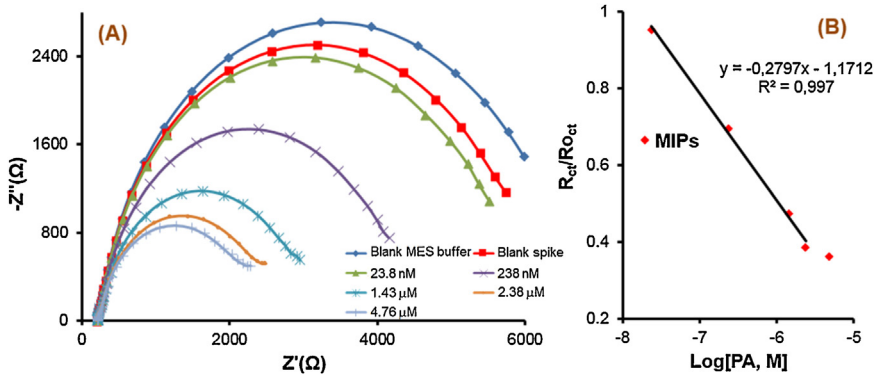

Fig. 6. EIS measurements of (A) MIPs based sensor and the corresponding calibration curves (B) in 5.0 mM $[Fe(CN)_6]^{3-}$ and 5.0 mM $[Fe(CN)_6]^{4-}$ by spiking PA in tap water.

3.6. Selectivity

The selectivity of the sensor was evaluated by EIS measurements using the competitive method [28]. In this case, the time and conditions were set as like the calibration of the sensors, and BSA was chosen to check the interferences as a model protein. Negligible interference effect was found, with a signal variation of only 1.7% when the PA and BSA concentration ratio was 1:0.1, and 0.35%, when the PA and BSA concentration ratio was 1:1(Fig. 5).

3.7. Application to real samples

Tap water, as a general source of bacteria, was selected as a proof-of-concept for the detection of PA. We spiked PA in tap water (tap water four times diluted in MES buffer) and checked the performance of the sensors. Using this matrix, the LOD is 16.83 nM (Fig. 6) which is a little bit higher than when detecting PA in pure MES buffer. This probably indicates that some inorganic ions may have some impact on the sensors performance by electrostatic interaction with the protein rebinding site or with the target protein.

We tested the recovery factors after spiking of PA in tap water. The spiked value was 2.38 μM and the recovered value was 2.17 μM, what means a recovery value of 91.08% with a standard deviation (calculated from the propagation of errors from the regression line) of 6.60%.

4. Conclusions

In this paper we present a molecularly imprinting-based analytical device for the direct electrical detection of the PA from *S. aureus.* This device concerns a simple and low cost assembly. It displays a good precision, selectivity, low detection limit, offering also the advantages of disposability, simple instrumentation and easy preparation for the detection of PA from the outer surface of *S. aureus*. This device can be seen as a first step for the detection of bacteria using molecularly imprinted polymer-based devices. Before using the device in field-conditions, further experiments are necessary to ensure its successful application to water holding bacterial contamination.

Acknowledgements

Catalan Government and European Research Council are acknowledged for the financial support of MARK PhD Fellowship (2013FI-B00842) and Starting Grant, 3P's, GA 311086 respectively. The URV team thanks the financial support from the Spanish Ministerio de Economía y Competitividad (Project CTQ2010-18717).

Appendix A. Supplementary data

Supplementary data associated with this article can be found, in the online version, at http://dx.doi.org/10.1016/j.snb.2016.04.075.

References

[1] D. Sompolinsky, Z. Samra, W.W. Karakawa, W.F. Vann, R. Schneerson, Z. Malik, Encapsulation and capsular types in isolates of *Staphylococcus aureus* from different sources and relationship to phage types, J. Clin. Microbiol. 22 (1985) 828–834.

[2] M.I. Halpin-Dohnalek, E.H. Marth, *Staphylococcus aureus*: production of extracellular compounds and behavior in foods—a review, J. Food Prot. 52 (1989) 267–282.

[3] T.E. Minor, E.H. Marth, Staphylococci and Their Significance in Foods, Elsevier Scientific Publishing Inc., Amsterdam, 1976.

[4] T. Lofkvist, J. Sjoquist, Chemical and serological analysis of antigen preparations from *Staphylococcus aureus*; a comparison between the products obtained by Verwey's and Jensen's techniques, Acta Pathol. Microbiol. Scand. 56 (1962) 295–304.

[5] T.C. Chang, S.H. Huang, Evaluation of coagulase activity and protein A production for the identification of *Staphylococcus aureus*, J. Food Prot. 58 (1995) 858–862.

[6] J. Movitz, Formation of extracellular protein A by *Staphylococcus aureus*, Eur. J. Biochem. 68 (1976) 291–299.

[7] J. Sjoquist, J. Movitz, I.-B. Johansson, H. Hjelm, Localization of protein a in the bacteria, Eur. J. Biochem. 30 (1972) 190–194.

[8] J.F. Song, X.F. Kang, W. Guo, Determination of hemoglobin in plasma and serum by linear-sweep polarography, Fresen. J. Anal. C. 357 (1997) 127–129.

[9] C. Anaya, N. Church, J.P. Lewis, Detection and identification of bacterial cell surface proteins by fluorescent labeling, Proteomics 7 (2007) 215–219.

[10] H. Zhu, S. Pan, S. Gu, E.M. Bradbury, X. Chen, Amino acid residue specific stable isotope labeling for quantitative proteomics, Rapid Commun. Mass Spectrom. 16 (2002) 2115–2123.

[11] K. Hempel, J. Pane, A. Otto, S. Sievers, M. Hecker, Quantitative cell surface proteome profiling for sigB-Dependent protein expression in the human pathogen *staphylococcus aureus* via biotinylation approach research articles, J. Proteome Res. 9 (2010) 1579–1590.

[12] Harold Tjalsma, Lambert Lambooy, Peter W. Hermans, Dorine W. Swinkels, Shedding & shaving: disclosure of proteomic expressions on a bacterial face, Proteomics 8 (2008) 1415–1428.

[13] D.J. Cahill, Protein and antibody arrays and their medical applications, J. Immunol. Methods 250 (2001) 81–91.

[14] A. Burkovski, Rapid detection of bacterial surface proteins using an enzyme-linked immunosorbent assay system, J. Biochem. Biophys. Methods 34 (1997) 69–71.

[15] N. Masqué, R.M. Marcé, F. Borrull, New polymeric and other types of sorbents for solid-phase extraction of polar organic micropollutants from environmental water, TrAC—Trends Anal. Chem. 17 (1998) 384–394.

[16] A.G. Mayes, K. Mosbach, Molecularly imprinted polymers: useful materials for analytical chemistry? TrAC—Trends Anal. Chem. 16 (1997) 321–332.

[17] Y. Lv, T. Tan, F. Svec, Molecular imprinting of proteins in polymers attached to the surface of nanomaterials for selective recognition of biomacromolecules, Biotechnol. Adv. 31 (2013) 1172–1186.

[18] E. Verheyen, J.P. Schillemans, M. van Wijk, M.-A. Demeniex, W.E. Hennink, C.F. van Nostrum, Challenges for the effective molecular imprinting of proteins, Biomaterials 32 (2011) 3008–3020.

[19] G. Vasapollo, R. Del Sole, L. Mergola, M.R. Lazzoi, A. Scardino, S. Scorrano, et al., Molecularly imprinted polymers: present and future prospective, Int. J. Mol. Sci. 12 (2011) 5908–5945.

[20] C. Algieri, E. Drioli, L. Guzzo, L. Donato, Bio-Mimetic sensors based on molecularly imprinted membranes, Sensors 14 (2014) 13863–13912.

[21] M.J. Whitcombe, I. Chianella, L. Larcombe, S.A. Piletsky, J. Noble, A. Horgan, The rational development of molecularly imprinted polymer-based sensors for protein detection, Chem. Soc. Rev. 40 (2011) 1547–1571.

[22] O. Hayden, P.A. Lieberzeit, Selective microorganism detection with cell surface imprinted polymers, Adv. Mater. 13 (2001) 1480–1483.

[23] O. Hayden, P.A. Lieberzeit, D. Blaas, F.L. Dickert, Artificial antibodies for bioanalyte detection — sensing viruses and proteins adv, Funct. Mater. 16 (2006) 1269–1278.

[24] K. Eersels, B. Van Grinsven, A. Ethirajan, S. Timmermans, J.F.J. Bogie, S. Punniyakoti, et al., Selective identi fi cation of macrophages and cancer cells based on thermal transport through surface-Imprinted polymer layers, ACS Appl. Mater. Interfaces 5 (2013) 7258–7267.

[25] S.A. Piletsky, S. Alcock, A.P.F. Turner, Molecular imprinting: at the edge of the third millennium, Trends Biotechnol. 19 (2001) 9–12.

[26] T.S.C.R. Rebelo, C. Santos, J. Costa-Rodrigues, M.H. Fernandes, J.P. Noronha, M.G.F. Sales, Novel Prostate Specific Antigen plastic antibody designed with charged binding sites for an improved protein binding and its application in a biosensor of potentiometric transduction, Electrochim. Acta. 132 (2014) 142–150.

[27] S.A.A. Almeida, L.A.A.N.A. Truta, R.B. Queirós, M.C.B.S.M. Montenegro, A.L. Cunha, M.G.F. Sales, Optimizing potentiometric ionophore and electrode design for environmental on-site control of antibiotic drugs: application to sulfamethoxazole, Biosens. Bioelectron. 35 (2012) 319–326.

[28] F.T.C. Moreira, S. Sharma, R.A.F. Dutra, J.P.C. Noronha, A.E.G. Cass, M.G.F. Sales, Protein-responsive polymers for point-of-care detection of cardiac biomarker, Sens. Actuators B. Chem. 196 (2014) 123–132.

[29] P.S. Sharma, A. Pietrzyk-le, F. D'souza, W. Kutner, Electrochemically synthesized polymers in molecular imprinting for chemical sensing, Anal. Bional. Chem. 402 (2012) 3177–3204.

[30] R. Tucceri, A.P.A. Scian, Electrosynthesis and spectroscopic characterization of poly(o-Aminophenol) film electrodes, ISRN Polym. Sci. 2012 (2012) (26 pages).

[31] J.S. Daniels, N. Pourmand, Label-Free impedance biosensors: opportunities and challenges, Electroanalysis 19 (2007) 1239–1257.

[32] I.I. Suni, Impedance methods for electrochemical sensors using nanomaterials, TrAC—Trends Anal. Chem. 27 (2008) 604–611.

[33] S.J. Ding, B.W. Chang, C.C. Wu, M.F. Lai, H.C. Chang, Impedance spectral studies of self-assembly of alkanethiols with different chain lengths using different immobilization strategies on Au electrodes, Anal. Chim. Acta. 554 (2005) 43–51.

[34] S.J. Ding, B.W. Chang, C.C. Wu, M.F. Lai, H.C. Chang, Electrochemical evaluation of avidin-biotin interaction on self-assembled gold electrodes, Electrochim. Acta 50 (2005) 3660–3666.

[35] T. Gopalasamy, M. Gopalswamy, M. Gopichand, J. Raj, Poly meta-Aminophenol: chemical synthesis, characterization and Ac impedance study, J. polym. 2014 (2014) 11pages.
[36] D.L. Franco, A.S. Afonso, S.N. Vieira, L.F. Ferreira, R. a. Gonçalves, A.G. Brito-Madurro, et al., Electropolymerization of 3-aminophenol on carbon graphite surface: electric and morphologic properties, Mater. Chem. Phys. 107 (2008) 404–409.
[37] S.K. Verma, P. Kar, D.J. Yang, A. Choudhury, Poly(m-aminophenol)/functionalized multi-walled carbon nanotube nanocomposite based alcohol sensors, Sens. Actuators B Chem. 219 (2015) 199–208.